BNL-113588-2017-JA

Self-Assembled Fe-N-Doped Carbon Nanotube Aerogels with Single-Atom Catalyst Feature as High-Efficiency Oxygen Reduction Electrocatalysts

Chengzhou Zhu, Shaofang Fu, Junhua Song, Qiurong Shi, Dong Su, Mark H. Engelhard, Xiaolin Li, Dongdong Xiao, Dongsheng Li, Junzheng Chen, Luis Estevez, Dan Du, and Yuehe Lin

Accepted by Small

February 2017

Center for Functional Nanomaterials

Brookhaven National Laboratory

U.S. Department of Energy
USDOE Office of Science (SC),
Basic Energy Sciences (SC-22)

DISCLAIMER

DOI: 10.1002/((please add manuscript number))
Article type: Communication

Self-Assembled Fe-N-Doped Carbon Nanotube Aerogels with Single-Atom Catalyst Feature as High-Efficiency Oxygen Reduction Electrocatalysts

*Chengzhou Zhu, Shaofang Fu, Junhua Song, Qiurong Shi, Dong Su, Mark H. Engelhard, Xiaolin Li, Dongdong Xiao, Dongsheng Li, Junzheng Chen, Luis Estevez, Dan Du, and Yuehe Lin**

[*] Dr. C. Zhu, S. Fu, J. Song, Q. Shi, Prof. D. Du, Prof. Y. Lin
School of Mechanical and Materials Engineering, Washington State University, Pullman, WA 99164, USA
E-mail: yuehe.lin@wsu.edu
Prof. Y. Lin, M. Engelhard, Dr. D. Xiao, Dr. D. Li,
Environmental Molecular Science Laboratory, Pacific Northwest National Laboratory, Richland, WA 99354, USA
Dr. X. Li, Dr. J. Chen, Dr. L. Estevez
Energy and Environmental Directory, Pacific Northwest National Laboratory, Richland, WA 99354, USA
Dr. D. Su
Center for Functional Nanomaterials, Brookhaven National Laboratory, Upton, New York 11973, USA
C. Zhu and S. Fu contributed equally to this work.

Keywords: Aerogels. transition metal–nitrogen–carbon structures. single-atom catalysts. nonprecious metal catalysts. oxygen reduction reaction

Finely controlled synthesis of high active and robust non-precious metal catalysts with excellent catalytic efficiency for oxygen reduction reaction (ORR) is extremely vital for successful implementation of fuel cells and metal batteries. Unprecedented ORR electrocatalytic performances and the diversified synthetic procedure in term of favorable structure/morphology characteristics make transition metals-derived M–N–C (M=Fe or Co) structures the most promising nanocatalysts. Herein, using the nitrogen-containing small molecular and inorganic salt as precursors and ultrathin tellurium nanowires as templates, we for the first time successfully synthesized a series of well-defined M-N-doped carbon nanotube aerogels with single-atom dispersion through one-step hydrothermal route and subsequent facile annealing treatment. Taking advantage of the porous nanostructures, one-

dimensional building block as well as homogeneity of active sites and single-atom catalyst feature, the resultant Fe-N-doped carbon nanotube aerogels exhibited excellent ORR electrocatalytic performance even better than that of the commercial Pt/C in alkaline solution, having great potential in fuel cell applications.

The development of robust electrocatalysts for oxygen reduction reaction (ORR) is the highest priority for commercialization of fuel cells and other electrochemical energy devices.[1-3] The inherently sluggish reaction kinetics of the ORR makes Pt-based nanomaterials the most efficient catalysts currently due to their superior electrochemical performances.[4-6] Nevertheless, these noble metal-based nanocatalysts still suffer from the prohibitive cost and scarcity of Pt in nature, low stability, and also the issue of methanol crossover. To this end, rational design and synthesis of highly efficient non-precious metal catalysts (NPMCs) are thereby desperately needed and become a very important topic in this field.[7-10] Among them, transition metal–nitrogen–carbon (M–N–C, M = Fe, Co) based nanomaterials have been considered as the most promising class of NPMCs for ORR due to their high ORR activity in both alkaline and acidic media.[11-15] Although the nature of the active sites in M–N–C catalysts remains controversial in the scientific community, there is a consensus that the transition metal dopants enable them robust catalysts and both M–N moieties and nitrogen doping are critical for the enhanced ORR performance.[11,16,17] So far the existing approaches for synthesizing M–N–C catalysts typically involve careful optimization of nitrogen/metal precursors and carbon supports, followed by a tedious acidic leaching and further thermal treatment.[8] It should be pointed out that most of the reported M–N–C nanostructures are usually characterized by heterogeneous morphologies without accurate control of homogeneity of active sites. Specifically, nanoscale engineering of these NPMCs with single-atom catalysis nature showed great promise in ORR due to the lowest size limit

and full atom utility.[18-20] Therefore, the development of a facile approach to accurately design this kind of single-atom catalysts is greatly needed and still remain challenging.

Aside from the composition control, rational tuning of the 3D porous structured carbon-based materials is another effective way to enhance the ORR performance by affording a high surface area and abundant exposed active sites, faster mass transport/diffusion and electron-transfer path.[21-24] Two different synthetic approaches regarding this kind of porous M-N-C nanostructures were involved. As for the first method, porous M-N-C structures were obtained through annealing treatment of nitrogen and metal precursors in the presence of 3D templates such as mesoporous silica and silica nanoparticles.[25-27] For the other method, metal atoms are first well embedded within the porous templates. Both the M–N–C active sites and porous nanostructures can be easily produced through direct carbonization at high temperatures.[28,29] Despite these contributions, some critical issues should be addressed regarding the rational design of 3D porous precursors and complicated post-treatments. Due to the extremely low density, large surface area and high porosity, carbon-based aerogels have been an appealing class of nanomaterials and opens up fascinating options for the preparation of new functional electrode materials.[30-32] On this basis, creation of novel M–N–C aerogels with special and enhanced functions, especially the porous characteristic along with advantageous building blocks and uniform active site distribution at an atomic level, can offer enormous opportunities to develop more state-of-the-art ORR NPMCs that can potentially promote the development of fuel cells.

Herein, we developed an efficient and universal approach for synthesizing the Fe-N-doped carbon nanotube aerogels (CNTAs) using tellurium nanowires as hard templates in the presence of nitrogen-containing small molecule and inorganic salt (Scheme 1). For the first time, the evolution of homogeneity of active sites with single-atom catalyst feature and the creation of the CNTAs were simultaneously realized through one-step hydrothermal method and subsequent heat treatment. Capitalizing on the advanced compositional and structural

features, the as-prepared catalysts possessed excellent electrocatalytic performance for ORR and even outperforms commercial Pt/C catalyst. Because of the convenient and universal synthetic strategy, exceptionally improved ORR activity and durability, this kind of Fe-N-doped may find potential application in fuel cells.

The one-step hydrothermal approach was adopted to synthesize CNTAs precursor in aqueous solution at 180 °C for 15 hr in the presence of well-defined tellurium nanowires, glucosamine hydrochloride and ammonium iron (II) sulfate with a mole ratio of 5. More detailed synthetic procedure is presented in supporting information. The resultant hydrogel precursor was soaked in distilled water to remove impurities for several times and then freeze dried. Finally, after thermal treatment at 900°C for 2 h in nitrogen atmosphere, Fe-N-doped CNTAs (Fe-N-CNTAs-5-900) were obtained. Using tellurium nanowires as template and glucose as carbon precursor to synthesize carbon-based hydrogel was reported previously.[33] Similarly, it is proposed that the successive dehydration and polymerization of glucosamine triggered the formation of the nitrogen-containing carbonaceous matrix coated on the surface of tellurium nanowires. Meanwhile, the intermediate nanowires join together and finally self-assemble into 3D nanowire hydrogel at the specific concentration of tellurium nanowires and carbon precursor. In this hydrothermal process, metal ions interacted with hydroxyl and amino groups were well embedded within carbonaceous matrix, leading to the homogeneous distribution of metal ions within N-doped carbon nanowires.[34-36] It should be noted that the metal ions (Fe, Co and Ni) homogenous doping and the creation of 3D nitrogen containing nanowires can be realized simultaneously through one-step hydrothermal approach, which significantly simplifies the catalyst preparation and enables the homogeneity of active sites within catalysts.

The morphology of the resultant Fe-N-CNTAs-5-900 was first investigated by scanning electron microscope (SEM) and transmission electron microscopy (TEM). As shown in Figure 1A, a highly porous nanowire network with fairly uniform in size and shape without

other byproducts was observed, leading to the low density of about 1.5 mg cm^{-3} (Figure S1). TEM analysis was further conducted and the result was shown in Figure 1B, C. It is found that interconnected CNTs with a diameter of 45 nm constitute the obtained aerogel. Moreover, it was found that hollow nanowires with a diameter of 10 nm can be efficient yielded as tellurium nanowires are volatile at high temperature and can be eliminated during pyrolysis (Figure S2). Different from the previously M-N-C structures derived from the direct annealing treatment of nitrogen and metal containing precursors, homogeneity of composition with slightly smooth surface instead of distinct aggregated nanoparticles of iron species (e.g., metallic iron, oxides or carbides) embedded within carbon nanostructures was presented, which can be confirmed by high-resolution TEM (HRTEM and corresponding high-angle annular dark-field scanning TEM (HAADF-STEM) images (Figure 1D, E). The ring-like selected area electron diffraction (SAED) pattern also demonstrated its poor crystallinity (Figure 1D). Moreover, elemental mapping images verify the existence and highly homogeneous distribution of C, N and Fe atoms in the obtained Fe-N-CNTAs-5-900 (Figure 1G). To illustrate the atomic structure of the Fe-N-C, high-resolution HAADF-STEM images were provided (Figure 1H, I). Several isolated bright dots, corresponding to heavier Fe atoms, could be well discerned in the carbon nanotube due to the different Z-contrast between Fe and C. The small size of these dots in the range of 0.2-0.3 nm further reveals the uniform dispersion of the individual Fe atom rather than Fe cluster and small crystals. As expected, the similar morphologies were also observed when the mole ratio between glucosamine hydrochloride and ammonium iron (II) sulfate varied. The introduction of Fe has no effect on the resultant product in comparison to N-CNTAs-900 (Figure S3). As such, taking advantage of the great versatility for the synthesis of this kind of materials, Co-N-CNTAs and Ni-N-CNTAs were also obtained with the similar structural characteristics (Figure S4).

X-ray diffraction (XRD) was conducted to further analyze their crystal structure (Figure 2A). No other diffraction peak was found except two distinct characteristic peaks at $2\theta = 26.5$ and

43° ascribing to (002) and (101),[37] regardless of the pyrolysis temperature. This result is consistent with the TEM analysis mentioned above. Furthermore, X-ray photoelectron spectroscopy (XPS) was used to reveal the detailed chemical composition of the resultant Fe-N-CNTAs-5 (Figure 2B-D). Survey scans of Fe-N-CNTAs at different annealing temperatures confirm the existence of C, N, O and Fe. Interestingly, we did not find the existence of Te in these final Fe-N-CNTAs, further verifying the fact that tellurium nanowires were completely removed at high temperatures and contributed to the evolution of the hollow structures, which was much simpler than previous reports on the removal of Te nanowires.[38] The C, N, O, and Fe contents in Fe-N-CNTAs-5-900 were determined to be 92.49, 2.06, 5.37, and 0.09 at%, respectively. The nitrogen content decreased from 4.51% to 2.06% with increasing heating temperature from 700 °C to 900 °C (Table S1). The high-resolution N1s spectrum of all Fe-N-CNTAs-5-900 can be deconvoluted into three different peaks at 398.3, 399.9, and 400.9 eV, corresponding to pyridinic-N/Fe-N, pyrrolic-N, and graphitic-N, respectively (Figure 2D).[39-41] It is worth noting that the peak located at 398.3 eV is also ascribed to nitrogen bound to the metal (Fe−N) because of the small difference in binding energy between N−Fe and pyridinic-N.[18, 25] Among them, 27% and 67.6% N atoms are in the form of pyridinic-N and graphitic-N, respectively, and some of the pyridinic-N atoms are bonded with Fe. These dominated nitrogen-containing compositions are believed to be served as the ORR active sites.[42]

To obtain the information on the surface area and porosity properties of the final product, N_2 physisorption measurement was carried out. As shown in Figure 2E, the Brunauer–Emmett–Teller (BET) surface area and pore volume of Fe-N-CNTAs-5-900 were 638.5 $m^2 g^{-1}$ and 1.6 $cm^3 g^{-1}$, respectively. The pores size distribution curve further indicated their hierarchically porous nanostructures with abundant mesopores (Figure 2F). This novel nanomaterial characterized by large surface area and pore volume can not only make more catalytic active

sites accessible but also guarantee faster electron transfer and mass transport, enabling them very promising in electrocatalysis.

Due to the unique nanostructured and compositional features (large surface area, 1D nanotube building block and homogeneity of active sites with single-atom catalyst feature) of resultant 3D porous Fe-N-CNTAs, they are expected to be excellent ORR catalysts. To evaluate the electrocatalytic activities for ORR, we first carried out cyclic voltammetry (CV) measurements on these newly designed Fe-N-CNTAs-5-900 in 0.1 M KOH solution in comparison with N-CNTAs-900 and commercial Pt/C (Figure 3A). In contrast to the virtually featureless CV curves within the entire potential range in N_2-saturated solution, the well-defined cathodic peaks appeared in all the CV curves of the three samples in the O_2-saturated solution. Compared with N-CNTAs-900 and Pt/C catalysts, Fe-N-CNTAs-5-900 showed much more positive ORR peak (0.897 V) than N-CNTAs-900 (0.777 V) and Pt/C (0.858 V). Comparison of the ORR activity of the prepared catalysts and gaining further insight into the ORR process was studied using RDE measurement at a scan rate of 10 mV s^{-1} and was demonstrated in Figure 3B. It is clear that the Fe-N-CNTAs-5-900 exhibited a satisfactory onset potential and half-wave potential (0.97 and 0.88 V), which is more positive than that of N-CNTAs-900 (0.91 and 0.84 V) and comparable to that of Pt/C (0.96 and 0.86 V). Furthermore, the Fe-N-CNTAs-5-900 afforded a large diffusion-limiting current, which was superior to the N-CNTAs-900 and Pt/C. The effect of annealing temperature on the catalyst activity for ORR was studied. Although all of them present the same morphology (Figure S5), we found that annealing temperature plays a critical role in the ORR activity and the obtained Fe-N-CNTAs-5-900 possessed the best ORR activity in term of the high onset potential and limited current density (Figure S6A, B). The ORR performance at Fe-N-CNTAs-5-900 was proposed to be closely associated with the improved electrochemically active surface area (EASA) and carbon crystallinity. To shed light on the enhanced ORR performance, EASA was investigated, which is closely associated with ORR activity. Figure S6C shows the

typical CV curves of different Fe-N-CNTAs-5 curves in N_2-saturated 0.1 M KOH solution. Among them, Fe-N-CNTAs-5-900 possesses the highest capacitance associated with current density, indicative of the largest EASA and more accessibility of the surface of the carbon nanostructures.[43] Raman spectra were also provided in Figure S6D. The D (≈1356 cm^{-1}) and G (≈1580 cm^{-1}) bands are ascribed to the disordered carbon (sp^3) and ordered graphitic carbon (sp^2), respectively.[44] The nature of carbon regarding the intensity ratio of D- and G-bands (I_D/I_G) suggested that Fe-N-CNTAs-5-900 afford a lower I_D/I_G value and therefore a more ordered graphitic carbon structure and higher conductivity. The other synthesis parameter that affects the ORR performance is the mass ratio between glucosamine hydrochloride and ammonium iron sulfate. As shown in Figure S7, the optimized ORR catalyst was obtained when the mole ratio between glucosamine hydrochloride and ammonium iron sulfate was 5. Besides, metal doping-dependent ORR behavior indicated that Fe-N-CNTAs-5-900 possessed high ORR activity in comparison to the Co and Ni-based samples (Figure S8).

The Tafel curves of the catalysts were also displayed to assess the unique structural and compositional advantages of Fe-N-CNTAs-5-900 (Figure 3C). In the potential region studied, the Fe-N-CNTAs-5-900 showed a Tafel slope of 87.8 mV dec^{-1}, almost the same with that of Pt/C catalysts, illustrating a good kinetic process for ORR. Only 0.09 at% Fe doping make the resultant catalyst more active, further demonstrating the highly efficiency of the Fe-N-C active site compared with N-doped counterpart. This finding further confirms the extreme efficiency of single atomic iron within the N-doped catalysts and provides the powerful guidance for synthesizing high rate ORR catalysts at single atom level. As shown in Figure 3D, the RDE polarization curves at various rotating speeds and corresponding Koutecky–Levich (K–L) plots of Fe-N-CNTAs-5-900 at different applied potentials were provided. Accordingly, the electron transfer number (n) of Fe-N-CNTAs-5-900 was calculated to be ~4.0 at 0.4–0.7 V (Figure 3E), suggesting a mainly 4e oxygen reduction process. The

significantly enhanced kinetic current densities (j_k) of the Fe-N-CNTAs-5-900 were also observed at the potential range investigated. Remarkably, the calculated j_k is 131.4 mA cm^{-2} at 0.4 V, which was about 2.85-fold of Pt/C (46.1 mA cm^{-2}). The methanol crossover effects and durability were also investigated. As expected, the Fe-N-CNTAs-900 showed better long-term stability (Figure 3F) and tolerance to methanol crossover effect (Figure S9) than Pt/C. Significantly, TEM images in Figure S10 reveal that the structure of nanowires was well maintained after stability test, while Pt/C catalyst showed obvious aggregations, confirming the better stability of Fe-N-CNTAs-5-900 during electrochemical process. Taken together, the porous structures characterized by unique hollow nanowire network provided the large surface area and abundant exposed active sites, promoting the mass transport and electron transfer. Uniform single-atom distribution of Fe ions within carbon matrix guarantees the homogeneity of active components, enhancing the catalytic efficiency of the catalyst. Both favorable factors render Fe-N-CNTAs a promising ORR electrocatalyst for fuel cells. Furthermore, it is expected that this unique single-atom Fe-N-C catalysts may provide a novel model to extensively study their ORR mechanism because of the unity of the electrocatalytic active sites.

In conclusion, we have demonstrated an efficient and versatile strategy for the creation of atomically dispersed M-N-CNTAs nanostructures. For the first time, the uniform distribution of metal ions within carbon matrix and the evolution of carbon nanotube hydrogels can be realized simultaneously through one-step hydrothermal approach. Subsequent annealing treatment gives rise to the M-N-CNTAs characterized by advanced features including porous nanotube networks and homogeneity of active sites with single atom catalyst feature. The newly designed Fe-N-CNTAs can be directly used as active and robust NPMCs for ORR without complicated post-treatment. Significantly, this novel single-atom electrocatalyst shows excellent ORR activity and much better stability than the Pt/C catalysts in alkaline medium, making it one of the most promising NPMCs.

Supporting Information
Supporting Information is available from the Wiley Online Library or from the author.

Acknowledgements
This work was supported by a start-up fund of Washington State University, USA. The XPS analysis was performed using EMSL, a national scientific user facility sponsored by the Department of Energy's Office of Biological and Environmental Research and located at Pacific Northwest National Laboratory (PNNL). We acknowledge Franceschi Microscopy & Image Center at Washington State University for TEM measurements. PNNL is a multi-program national laboratory operated for DOE by Battelle under Contract DE-AC05-76RL01830.

Received: ((will be filled in by the editorial staff))
Revised: ((will be filled in by the editorial staff))
Published online: ((will be filled in by the editorial staff))

References

[1] M. K. Debe, *Nature* **2012**, *486*, 43.

[2] K. Gong, F. Du, Z. Xia, M. Durstock, L. Dai, *Science* **2009**, *323*, 760.

[3] C. Zhu, D. Du, A. Eychmüller, Y. Lin, *Chem. Rev.* **2015**, *115*, 8896.

[4] S. Guo, S. Zhang, S. Sun, *Angew. Chem., Int. Ed.* **201**3, *52*, 8526.

[5] S. Guo, S. Sun, *J. Am. Chem. Soc.* **2012**, *134*, 2492.

[6] Z. Chen, M. Waje, W. Li, Y. Yan, *Angew. Chem., Int. Ed.* **2007**, *46*, 4060.

[7] W. Yang, X. Liu, X. Yue, J. Jia, S. Guo, *J. Am. Chem. Soc.* **2015**, *137*, 1436.

[8] G. Wu, P. Zelenay, *Acc. Chem. Res.* **2013**, *46*, 1878.

[9] L. Dai, Y. Xue, L. Qu, H.-J. Choi, J.-B. Baek, *Chem. Rev.* **2015**, *115*, 4823.

[10] H.-W. Liang, X. Zhuang, S. Brüller, X. Feng, K. Müllen, *Nat. Commun.* **2014**, *5*, 4973.

[11] G. Wu, A. Santandreu, W. Kellogg, S. Gupta, O. Ogoke, H. Zhang, H.-L. Wang, L. Dai, *Nano Energy* 2016, 29, 83.

[12] G. Wu, K. L. More, C. M. Johnston, P. Zelenay, *Science* **2011**, *332*, 443.

[13] M. Lefèvre, E. Proietti, F. Jaouen, J.-P. Dodelet, *Science* **2009**, *324*, 71.

[14] A. Serov, K. Artyushkova, P. Atanassov, *Adv. Energy Mater.* **2014**, *4*, 1301735.

[15] S. Fu, C. Zhu, H. Li, D. Du, Y. Lin, *J. Mater. Chem. A* **2015**, *3*, 12718.

[16] Q. Jia, N. Ramaswamy, H. Hafiz, U. Tylus, K. Strickland, G. Wu, B. Barbiellini, A. Bansil, E. F. Holby, P. Zelenay, S. Mukerjee, *ACS Nano* **2015**, *9*, 12496.

[17] A. Zitolo, V. Goellner, V. Armel, M.-T. Sougrati, T. Mineva, L. Stievano, E. Fonda, F. Jaouen, *Nat. Mater.* **2015**, *14*, 937.

[18] H. Fei, J. Dong, M. J. Arellano-Jimenez, G. Ye, N. Dong Kim, E. L. G. Samuel, Z. Peng, Z. Zhu, F. Qin, J. Bao, M. J. Yacaman, P. M. Ajayan, D. Chen, J. M. Tour, *Nat. Commun.* **2015**, *6*, 8668.

[19] B. Qiao, A. Wang, X. Yang, L. F. Allard, Z. Jiang, Y. Cui, J. Liu, J. Li, T. Zhang, *Nat. Chem.* **2011**, *3*, 634.

[20] P. Liu, Y. Zhao, R. Qin, S. Mo, G. Chen, L. Gu, D. M. Chevrier, P. Zhang, Q. Guo, D. Zang, B. Wu, G. Fu, N. Zheng, *Science* **2016**, *352*, 797.

[21] C. Zhu, H. Li, S. Fu, D. Du, Y. Lin, Chem. *Soc. Rev.* **2016**, *45*, 517.

[22] J. Tang, J. Liu, C. Li, Y. Li, M. O. Tade, S. Dai, Y. Yamauchi, *Angew. Chem., Int. Ed.* **2015**, *54*, 588.

[23] X. Wang, H. Zhang, H. Lin, S. Gupta, C. Wang, Z. Tao, H. Fu, T. Wang, J. Zheng, G. Wu, X. Li, *Nano Energy* **2016**, *25*, 110.

[24] S. Ma, G. A. Goenaga, A. V. Call, D.-J. Liu, *Chem. Eur. J.* **2011**, *17*, 2063.

[25] H.-W. Liang, W. Wei, Z.-S. Wu, X. Feng, K. Muellen, *J. Am. Chem. Soc.* **2013**, *135*, 16002.

[26] Y. Wang, A. Kong, X. Chen, Q. Lin, P. Feng, *ACS Catal.* **2015**, *5*, 3887.

[27] M. Zhou, C. Yang, K.-Y. Chan, *Adv. Energy Mater.* **2014**, *4*, 1400840.

[28] Q. Lin, X. Bu, A. Kong, C. Mao, F. Bu, P. Feng, *Adv. Mater.* **2015**, *27*, 3431.

[29] B. You, N. Jiang, M. Sheng, W. S. Drisdell, J. Yano, Y. Sun, *ACS Catal*. **2015**, *5*, 7068.

[30] H. W. Liang, Z. Y. Wu, L. F. Chen, C. Li, S. H. Yu, *Nano Energy* **2015**, *11*, 366.

[31] J. T. Zhang, Z. H. Zhao, Z. H. Xia, L. M. Dai, *Nat. Nanotechnol.* **2015**, *10*, 444.

[32] L. Chen, R. Du, J. H. Zhu, Y. Y. Mao, C. Xue, N. Zhang, Y. L. Hou, J. Zhang, T. Yi, *Small* **2015**, *11*, 1423.

[33] H.-W. Liang, Q.-F. Guan, L.-F. Chen, Z. Zhu, W.-J. Zhang, S.-H. Yu, *Angew. Chem., Int. Ed.* **2012**, *51*, 5101.

[34] G. Zhang, X. W. Lou, *Angew. Chem., Int. Ed.* **2014**, *126*, 9187.

[35] J. Wang, N. Yang, H. Tang, Z. Dong, Q. Jin, M. Yang, D. Kisailus, H. Zhao, Z. Tang, D. Wang, *Angew. Chem., Int. Ed.* **2013**, *52*, 6417.

[36] M.-M. Titirici, M. Antonietti, A. Thomas, *Chem. Mater.* **2006**, *18*, 3808.

[37] A. Kong, X. Zhu, Z. Han, Y. Yu, Y. Zhang, B. Dong, Y. Shan, *ACS Catal.* **2014**, *4*, 1793.

[38] L.-T. Song, Z.-Y. Wu, H.-W. Liang, F. Zhou, Z.-Y. Yu, L. Xu, Z. Pan, S.-H. Yu, *Nano Energy* **2016**, *19*, 117.

[39] J. Liang, X. Du, C. Gibson, X. W. Du, S. Z. Qiao, *Adv. Mater.* **2013**, *25*, 6226.

[40] W. He, C. Jiang, J. Wang, L. Lu, *Angew. Chem., Int. Ed.* **2014**, *53*, 9503.

[41] Y. Zhao, K. Watanabe, K. Hashimoto, *J. Am. Chem. Soc.* **2012**, *134*, 19528.

[42] L. Lai, J. R. Potts, D. Zhan, L. Wang, C. K. Poh, C. Tang, H. Gong, Z. Shen, J. Lin, R. S. Ruoff, *Energy Environ. Sci.* **2012**, *5*, 7936.

[43] S. Gupta, L. Qiao, S. Zhao, H. Xu, Y. Lin, S. V. Devaguptapu, X. Wang, M. T. Swihart, G. Wu, *Adv. Energy Mater.* **2016**, *6*, 1601198.

[44] C. Zhu, S. Guo, Y. Fang, S. Dong, *ACS Nano* **2010**, *4*, 2429-2437.

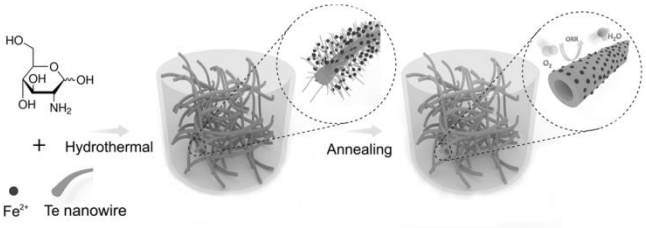

Scheme 1. Schematic illustration of the synthesis procedure of Fe-N-CNTAs.

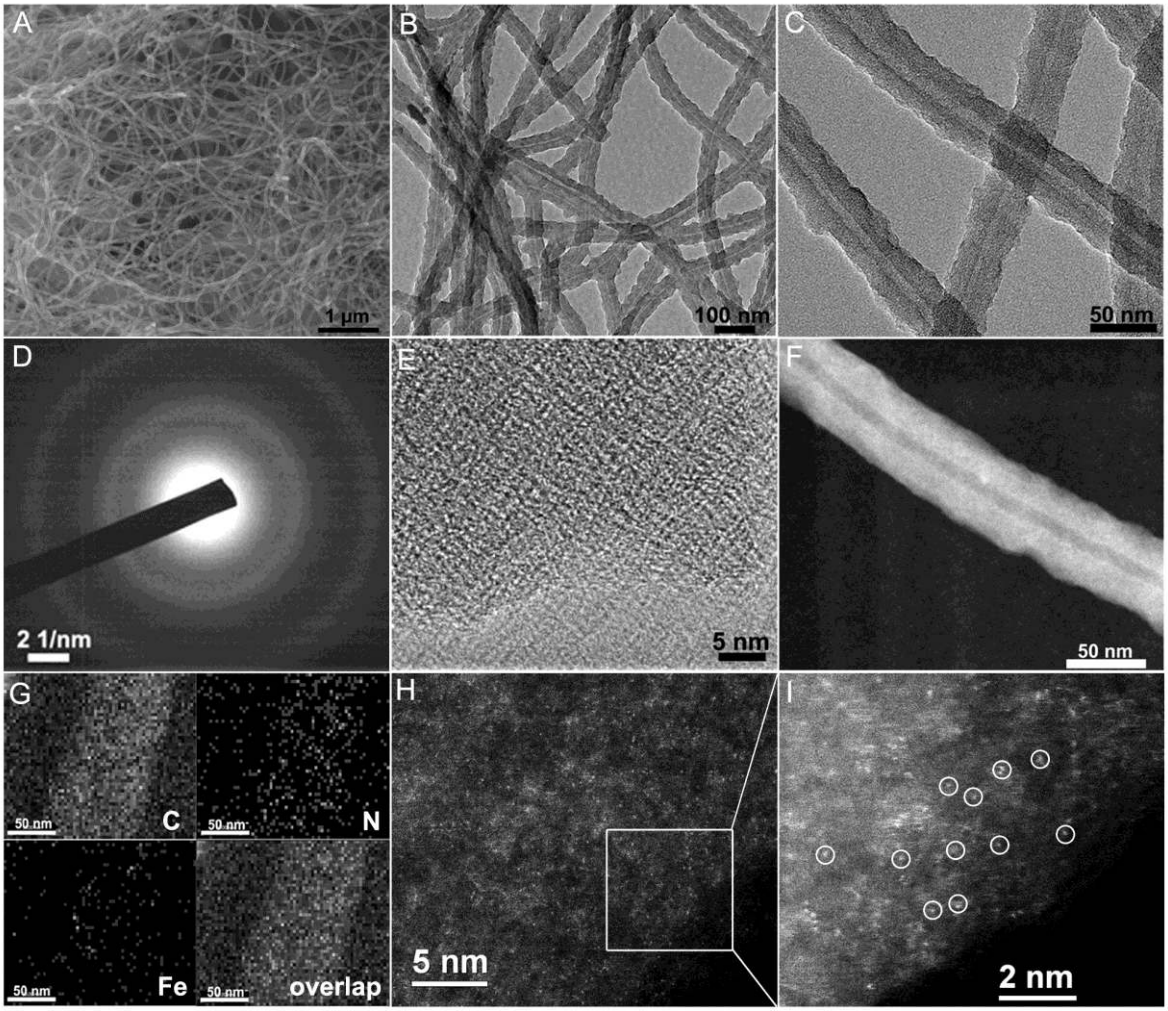

Figure 1. SEM (A), TEM (B, C), HRTEM (E) and HAADF-STEM (F, H and I) images of the obtained Fe-N-CNTAs-5-900. The selected area electron diffraction pattern (D) and elemental distribution of the C, N and Fe atoms in the obtained Fe-N-CNTAs-5-900.

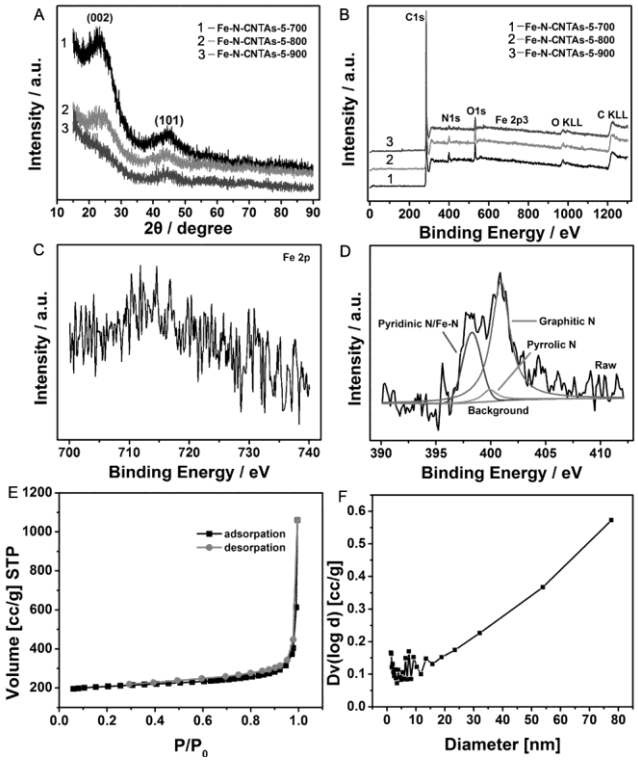

Figure 2. XRD (A) and XPS (B) spectra of Fe-N-CNTAs-5 annealed at different temperatures. XPS Fe 2p (B) and N 1s (D) spectra of the Fe-N-CNTAs-5-900. Nitrogen adsorption and desorption isotherms (E) and pore size distribution curve (F) of Fe-N-CNTAs-5-900.

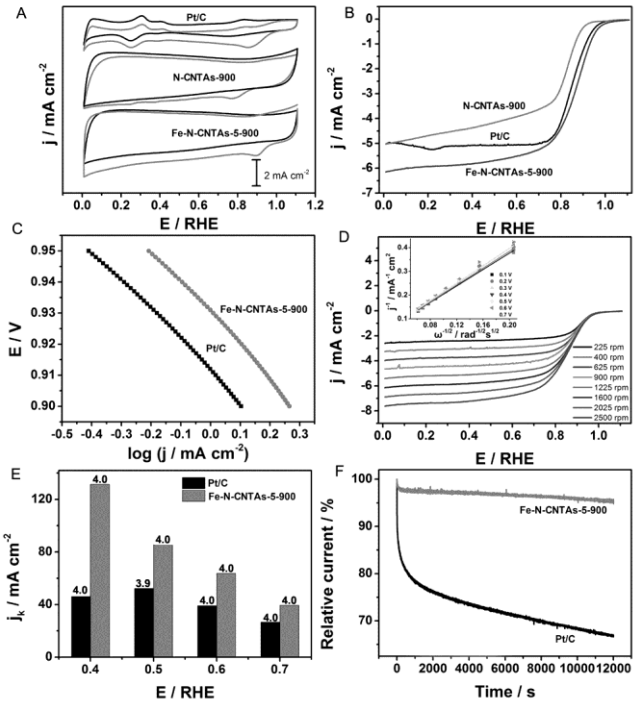

Figure 3. (A) CV curves of Fe-N-CNTAs-5-900, N-CHNAs-900 and commercial Pt/C in N_2- and O_2-saturated 0.1 M KOH solution. The scan rate was 50 mV s^{-1}. (B) RDE polarization curves of various catalysts in O_2-saturated 0.1 M KOH solution at a scan rate of 10 mV s^{-1} and a rotation rate of 1600 rpm. (C) Tafel plots derived from Figure 2B. (D) RDE polarization curves on Fe-N-CNTAs-5-900 at different rotation rates, inset: K–L plot of J^{-1} versus ω^{-1}. (E)

Kinetic current density (j_k) and the electron-transfer number (n) of the Fe-N-CNTAs-5-900 and Pt/C at different potentials. (F) Current versus time (i–t) chronoamperometric response of the Fe-N-CNTAs-5-900 and Pt/C at 0.7 V in O_2-saturated 0.1 M KOH at 200 rpm, respectively.

Self-assembled M-N-doped carbon nanotube aerogels with single-atom catalyst feature are for the first time reported through one-step hydrothermal route and subsequent facile annealing treatment. By taking advantage of the porous nanostructures, one-dimensional nanotubes as well as single-atom catalyst feature, the resultant Fe-N-doped carbon nanotube aerogels exhibit excellent ORR electrocatalytic performance even better than commercial Pt/C in alkaline solution.

Keyword Aerogels. transition metal–nitrogen–carbon structures. single-atom catalysts. nonprecious metal catalysts. oxygen reduction reaction

Chengzhou Zhu, Shaofang Fu, Junhua Song, Qiurong Shi, Dong Su, Mark H. Engelhard, Xiaolin Li, Dongdong Xiao, Dongsheng Li, Junzheng Chen, Luis Estevez, Dan Du, and Yuehe Lin*

Self-Assembled Fe-N-Doped Carbon Nanotube Aerogels with Single-Atom Catalyst Feature as High-Efficiency Oxygen Reduction Electrocatalysts

ToC figure